Supplementary Material to Excitonic fine structure in emission of linear carbon chains

Stella Kutrovskaya,[*,†,‡,¶] Anton Osipov,[¶,§] Stepan Baryshev,[‖] Anton Zasedatelev,[‖] Vladislav Samyshkin,[¶] Sevak Demirchyan,[†,‡] Olivia Pulci,[⊥] Davide Grassano,[⊥] Lorenzo Gontrani,[⊥] Richard Rudolph Hartmann,[#] Mikhail E. Portnoi,[@,△] Alexey Kucherik,[¶] Pavlos G. Lagoudakis,[‖] and Alexey Kavokin[†,‡,∇]

†*School of Science, Westlake University,Hangzhou 310024, China*

‡*Institute of Natural Sciences, Westlake Institute for Advanced Study, Hangzhou 310024, China*

¶*Department of Physics and Applied Mathematics, Stoletov Vladimir State University, Vladimir 600000, Russia*

§*ILIT RAS — Branch of FSRC "Crystallography and Photonics" RAS, Shatura 140700, Russia*

‖*Skolkovo Institute of Science and Technology, Moscow 121205, Russia*

⊥*Department of Physics, University of Rome Tor Vergata, I-00133 Rome, Italy*

#*Physics Department, De La Salle University, 0922 Manila, Philippines*

@*Physics and Astronomy, University of Exeter, Exeter EX4 4QL,United Kingdom*

△*ITMO University, St. Petersburg 197101, Russia*

∇*Spin Optics Laboratory, St. Petersburg State University, St. Petersburg 198504, Russia*

E-mail: stella.kutrovskaya@westlake.edu.cn

The synthesis of linear carbon chains in a liquid. We have used the method of laser fragmentation of colloidal carbon systems for realisation of stabilised carbon chains. To create carbon-gold bonds we additionally illuminated the solution by nanosecond laser pulses generated by an Ytterbium (Yb) fiber laser having the central wave length of 1.06 mm, the pulse duration of 100 ns, the repetition rate of 20 kHz and the pulse energy of up to 1 J. The time between subsequent pulses was about 1 s. The sizes of gold NPs have been controlled by the dynamic laser scattering device Horiba SZ100. The formation of polyyne carbon phase we have controlled on the Raman spectra measured by using the Senterra spectrometer, made by Bruker company. The pump laser wavelength is of 532 nm at the power level of 40 mW, the radiation was focused through a 50-fold microlens, the spectra were collected in the confocal microscope configuration and averaged over 10 measurements. The accumulation time of each measurement was 60 seconds. For the detailed study of the orientation distribution of nanodipoles, we have performed the high resolution transmission electron microscopy and X-ray diffraction studies using FEI Titan^3 with a spatial resolution of up to 2 Å . Processing of TEM-images and diffraction patterns was conducted with the opened database package Image J 1.52 a. We study the photoluminescence (PL) of carbon chains using the 140 fs pulsed 80 MHz repetition rate Ti: Sapphire laser system (Coherent Cameleon Ultra ll) coupled to an optical parametric oscillator allowing for fine control over the excitation energies. As the sample is mounted in a closed-cycle cryostation, Montana Instruments Cryostation C2, we carry out PL measurements in a vacuum within the temperature range of 4K-300K. The optical excitation we employ in these experiments is tightly focused onto a sample by Mitutoyo M Plan APO SL x50 microscope objective with a numerical aperture of 0.42. Note that we use three different excitation wavelengths to elucidate the nature of the observed fine lines in the PL spectra, namely 390, 380 and 370 nm as shown in Figure 3(b) of the main text. We collect PL signal in the transmission configuration using the same Mitutoyo M Plan APO SL x50 microscope objective. To avoid any parasitic signal in PL spectra we filter out optical excitation with a short pass filter

cutting light above 561nm, and in the collection path we use a long pass filter transmitting light above 400nm to get rid of the optical excitation signal. Being properly filtered, the PL from the sample is coupled into a 750 mm focal length spectrometer (Princeton Instruments SP2750) equipped with a charge-coupled device camera (Pixis-XB: 1024BR) with 1024x1024 imaging array. In all the spectroscopic measurements we use 1200 grooves mm^{-1} grating and 20 μm entrance slit, as well as step and glue technique to record the entire PL spectra represented in Figures 3 and 4 of the main text. The spectral resolution of our setup is 100 pm. Despite omnipresent background emission from the substrate (above 650 nm) we systematically observe several distinct peaks in the PL of the sample that correspond to the optical transitions of carbon chains of the different lengths. We further extend our spectroscopic analysis with in-depth study of the PL dynamics attributed to the identified optical transitions. We employ a standard time-correlated single-photon counting technique (TCSPC), with detection wavelengths scanned across the full emission bandwidth using a variable birefringent filter device (Liquid crystal tunable filter Varispec). The recorded spectra of the PL coupled to TCSPC system are shown in Figure 4a and Figure 4b of the main text. We extract spectral lines within 5 nm linewidth that corresponds to the exciton and trion transitions. We use a single-photon avalanche photodiode (APD) (id100-MMF50) together with TCSPC module (SPC-160, Becker & Hickel GMBH) to detect photon events related to the PL. The typical count rate is 10^3-10^4 counts/s while a dark count rate is 40 Hz. The APD response defines the time resolution in our system, which is as short as 60 ps. By using the aforementioned technique, we measure emission decay for five individual optical transitions (Figures 4a,b,c,d of the main text).

Fabrication and characterization. We employ here the method of synthesis of carbon chains which consists of two stages, as is also described in works.[1,2] At the first stage, we produce a colloidal solution of disoriented carbon clusters as a result of laser fragmentation of a carbon sample placed in a distilled water (fig.S1(a)). We chose shungite as a target because its original structure is composed of fragments of nonplanar graphene (NGr) with

sp^2-hybridization[3] and it is usually free from impurities.

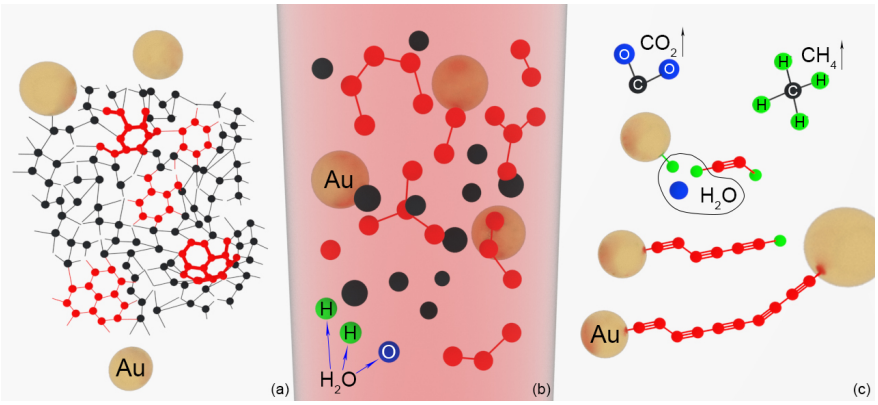

Figure S1: The synthesis of stable carbon chains. An illustration of the evolution of an amorphous shungite structure into an ensemble of carbon chains under the effect of laser irradiation: a) the initial mixed solution of the separated gold NPs, shown as yellow spheres and shungite components: the fragmentary crystalline phase depicted by red and amorphous carbon atoms shown in black. Atom vacancies are shown by empty circles; b) the laser-induced fragmentation of the *NGr* and local water decomposition into oxygen and hydrogen are shown as blue and green spheres, respectively; c) the schematics of the stabilization of liner carbon chains by gold nanoparticles. Gold NPs in these schematics are shown out of the scale.

The chemically imposed metamorphism of shungite makes it free from residual impurities and not susceptible to graphitization.[3] To stabilize long linear carbon chains in the distilled water solution we add spherical gold nanoparticles with an average size of either 10 nm or 100 nm (see. Fig. S1). This size estimate is confirmed by TEM images and is supported by the

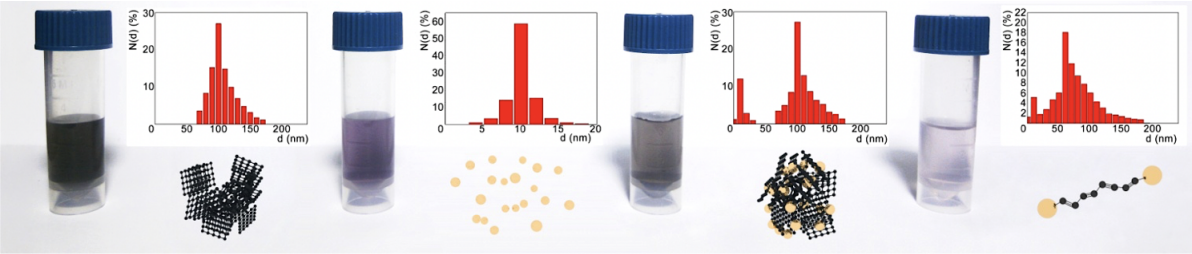

Figure S2: Colloidal systems of different compositions realized within the linear carbon synthesis procedure that we employed. Left to right: a) the initial carbon system, b) gold nanoparticles, c) the initial mixed solution, d) the mixed system after ns-laser pulse irradiation.

fact that NPs of 10 nm and 100 nm diameter demonstrate the Rayleigh shape stability[4] and

are transparent to the near infrared (NIR) laser light of 1.06 μm. Under the effect of laser action characterised by pulse energy up to 1 mJ,[1] the allotropic transition may be achieved in case of the appropriate choice of media parameters such as the pressure of about 10 GPa and the temperature up to 4000 K.[5] These laser-induced critical media parameters enable the thermal decomposition of water into hydrogen and oxygen in the mixed liquid system. The chemical activity of different forms of carbon is reduced as amorphous carbon transforms to textured sp^2-allotropes. First, the amorphous part of shungite is decomposed into free carbon atoms (see Fig. S1). Then the free carbon atoms either diffuse out of the volume heated by the laser irradiation to form C_2 molecules or react with oxygen and hydrogen to form volatile gases (CH_4, CO, CO_2, etc.). Due to the presence of defects, the distorted sp^2 - lattices start reacting with hydrogen at the temperature of 1200 °C.[6] Carbon's different hybridizations result in a huge class of carbon-based compounds, in particular, polymer chains.[7,8] Once out of the laser heating zone limited by the beam diameter of 30 μm and beyond the thermal diffusion length in water that is about 10 μm, hydrogen atoms accumulate on surfaces of gold particles due to the presence of free surface electrons (see Fig. S1 (b)) or form a single electron bond with the carbon materials organizing into the $C_x - H$ group.[8] On the other hand, hydrogen atoms may restore bonds with an oxygen atom resulting in the appearance of a water molecule. If there is a free fragment of the chain at a length that is sufficient to form a stable Van der Waals bond than an Au-C interface is formed through a single carbon bond.[8] By this mechanism, gold nanoparticles are capable of efficiently catalysing the growth of carbon by pulling the end carbon atoms into the crystal lattice of metal nanoparticles (NPs).[2,9] Since the activation energy of an electron in gold is sufficiently low, it leads to the formation of stable metal-carbon bonds. It is important to note that the gold anchors stabilize the long linear carbon chains (LLCCs) by preventing their vibration-induced decomposition into shorter components, folding and bending. A significant loss of color of the solution is characteristic of the phase transition (fig.S2 (a-d)). Linear carbon chains are stabilized by the effect of the environment in a colloidal solution and due to gold

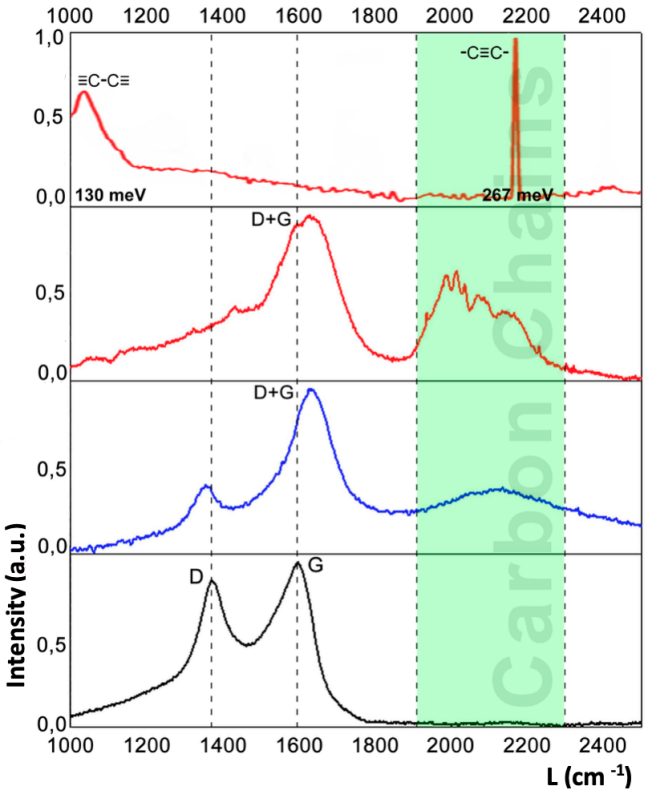

Figure S3: shows the Raman spectra of the solution at the different stages of the laser grown process. The bottom (black) curve represents the Raman spectrum of the initial shungite precursor in liquid, the blue curve corresponds to the unstabilized carbon threads in a solution, the bottom red curve shows the transformation of the Raman spectra at the beginning of carbon chains grown in the presence of gold nanoparticles. The peaks correspond to characteristic vibron modes of the isolated linear chains of various lengths. The resulting Raman spectrum of the solution containing gold-stabilized carbon chains is depicted with upper red curve. The peaks correspond to characteristic vibron modes of the polyyne allotrope.

NPs attached to the ends of the chains.

We analyzed the synthesized nanoparticles using the dynamic light scattering (DLS) at the Horiba LB-550 and explored the particle's size (exposition time was about 30 sec). These measurements showed how the dispersed phase of liquid systems varied during the process of synthesis. The particle's size distribution in a mixed system certifies of the presence of two non-interacting fractions: the smaller-size Au NPs and the parts of disordered carbon. With the increase of the processing time, the colloidal solution becomes colorless. The variation of the bimodal histogram (Fig. S2) in time evidences the interplay of two competitive

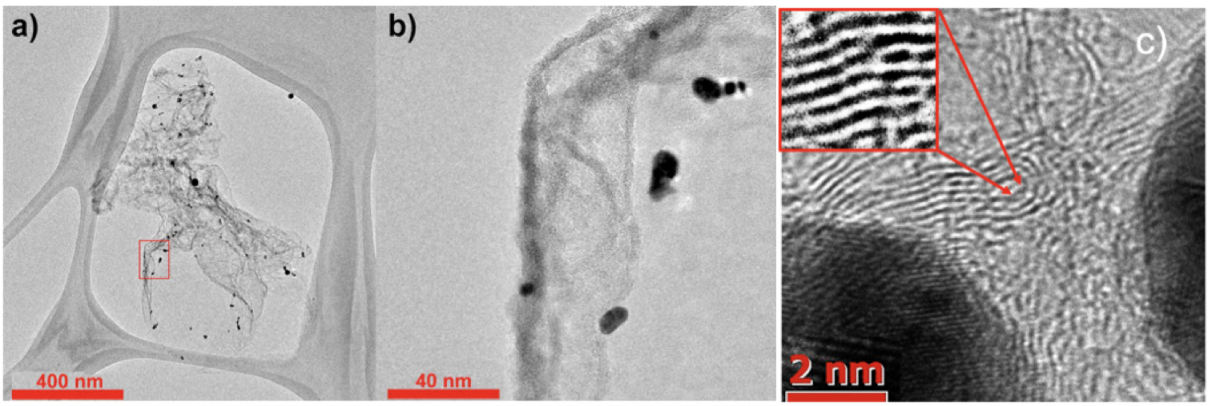

Figure S4: A microscopic quasi-1D structure revealed by TEM imaging. (a) shows the TEM image of a free-standing metal-carbon film attached to the gold-platinum grid; (b) is the magnified part of (a); (c) A characteristic high resolution TEM image of the linear carbon chains. The dark shadows correspond to the gold nanoparticles at their ends.

processes: the fragmentation of carbon compounds under the effect of laser radiation and their self-assembly into long liner chains formed in the peripheral volumes of the colloid. The evolution of carbon allotropes is also very apparent in the dramatic modification of the Raman spectra (Fig. S3). The resonance Raman spectroscopy was used to verify the optimal growth conditions for the bulk-yield synthesis of LLCCs. In this figure the Raman bands are interpreted in agreement with the earlier works.[10,11] We observed the degradation of defect-induced (D-band) and graphitic mode (G-band) during the laser action. The LLCCs exhibit a Raman active mode referred to as the LLCC-band.[12] Polyynes with fewer than 20 carbon atoms are characterised by bands between 1,900 and 2,300 cm^{-1}.[13] The resulting spectra corresponding to LLCCs endcapped with gold NPs don't show any signal characteristic of stretching modes in contrast to the hydrogen-capped oligoynes[11]. Traces of D- and G-bands are completely washed out in the top-spectrum of Fig. S3, which only shows the strong peaks characteristic of polyyne chains. This proves that sp-carbon phase dominates in our samples.

The laser preparation process leads to the formation of carbon thread attached to gold NPs. This can be very well seen using the high resolution transmission electron microscopy (HR TEM) of a deposited structure (see Fig. S4).

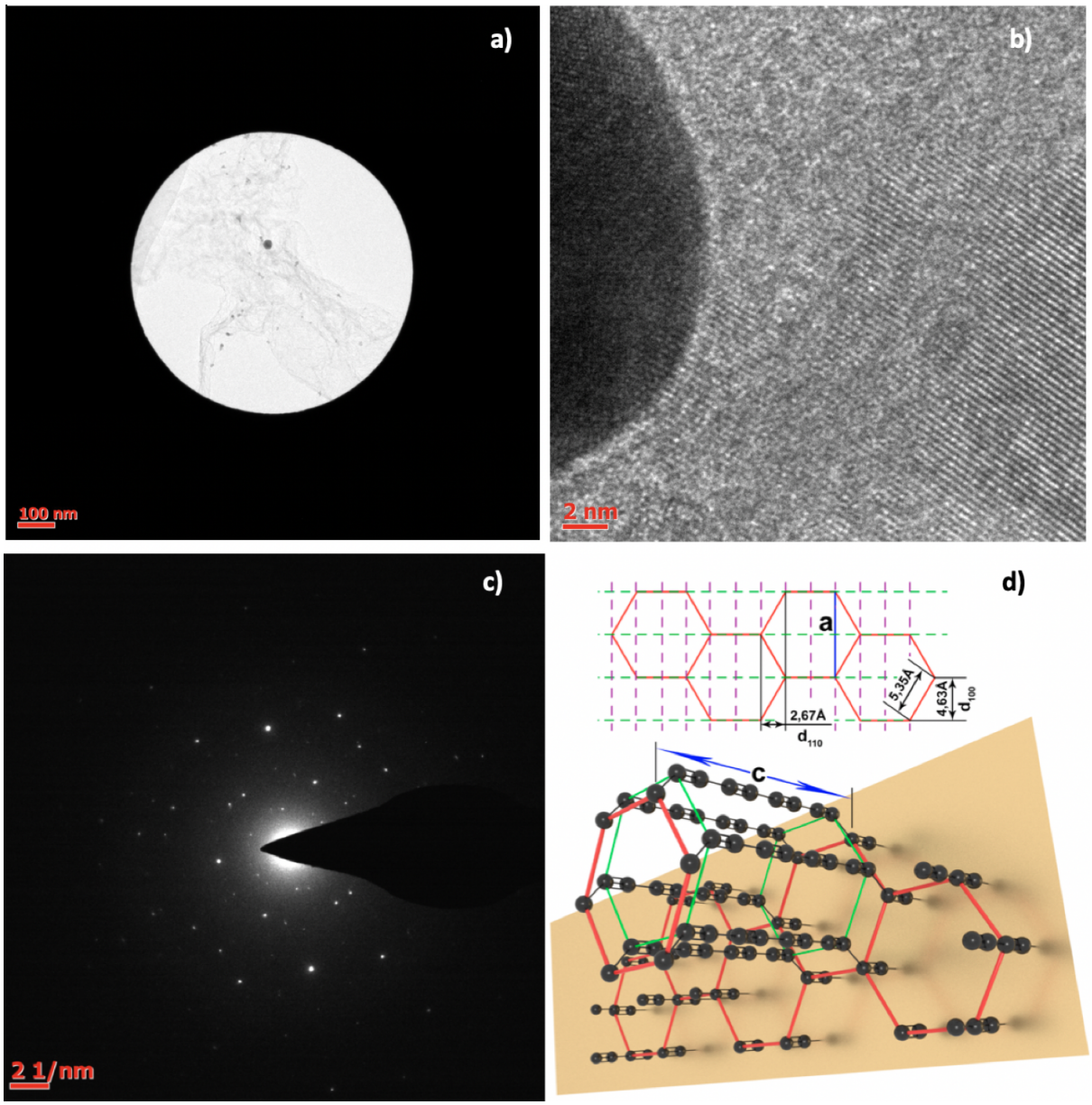

Figure S5: A microscopic quasi-1D structure. (a) The TEM image of the area for X-ray diffraction data collection; (b) The magnified part of a gold NP seen as a dark sphere that clearly shows the linear carbon chains attached to the surface of the gold NP; (c) the diffraction pattern of the deposited LLCC threads end-capped with Au NPs. (d) shows schematically the crystal structure of the synthesized linear carbon chains crystallines, self-organized via Van-der-Waals interaction between neighboring linear chains and attached to the surfaces of gold NPs.

To reveal the crystal structure of the obtained material we have used the X-ray diffraction technique.[14] The diffraction pattern was produced by a focused electron beam diffracted on the thin metal-carbon film in vacuum. Fig. S5 (a) shows the area of the sample examined in

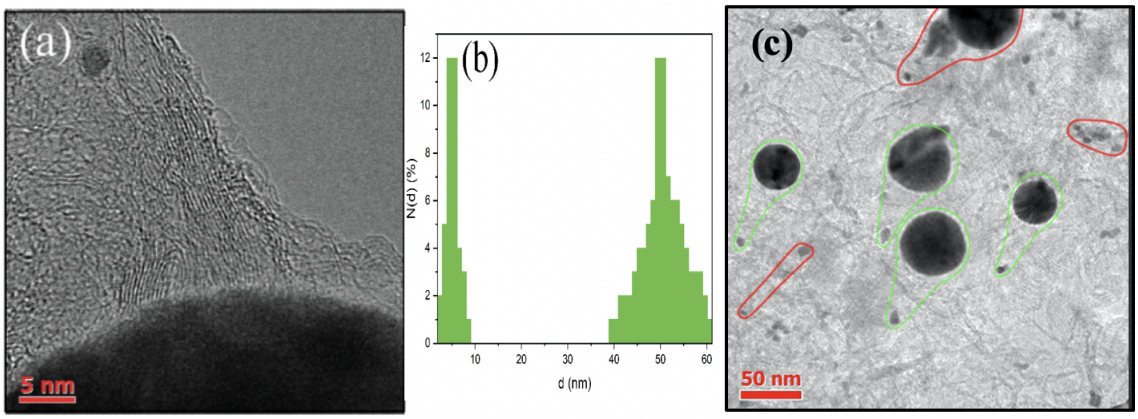

Figure S6: Experimental results on the deposition of the monoatomic carbon chains end-capped with Au NPs in the presence of the static electric field. (a) TEM image of the LLCC wire bundles tight between two NPs. The dark region at the bottom corresponds to the larger nanoparticle of a nearly spherical shape with the radius 25 nm. (b) the histogram of the NP size distribution. (c) shows the ensemble of closely spaced nanodipoles oriented along the field (marked by green curves). The NP-carbon wires complexes framed with red are insensitive to the electric field and are randomly oriented. Figure S6 is adapted from Ref.[14]

this X-ray study. Fig. S5(b) shows the observed diffraction pattern. The analysis of X-ray diffraction images allows to restore the full crystal structure of the deposited thin film. The observed diffraction pattern represents a system of point type reflexes (see fig.S5 (b)) that corresponds to a hexagonal lattice with a zone axis [001]. This indicates a high degree of the structure ordering in the studied sample. The specifically oriented hexagonal pattern is characteristic of quasi-1D LLCC crystallines oriented in the real space.[15] The measured interplanar distances d_{100} = 4.63 Å and d_{110} =2.67Å (see fig.S4 (c)) are very close to the values reported for hexagonal carbyne materials in.[16,17] Taking to account spatial group symmetry the carbon chains should self-organize to form a hexagon package as fig.S5(c) shows schematically. The linear carbon chains modification realized in the present work is characterized by lattice parameters of a=9.26 Å and c= 12.5 Å . In our case the distance between neighboring atoms is 5.35 Å in the hexagon, which is almost twice larger than the bond-length alternation 2.57 Å for the carbyne crystal studied in.[8] We argue that in our system the interaction between the chains must be relatively weak. Since the deposited

structure is a parallel array of carbon filaments, in the perpendicular direction the interaction between the filaments is provided by Van der Waals forces. The interchain distance must be one that minimizes the free energy of the array of the chains linked by Van der Waals interaction.[18,19] The presence of gold anchors at the ends stabilizes free standing quasi-1D structure in vacuum. The TEM image of the surface of a gold NP and multiple linear carbon chains attached to it is shown in Fig. S4 (c), S5 (b) and S6 (a). Fig. S6 (a,c) show that the lengths of carbon chains connecting gold NPs may be of 30-50 nm. The lengths of straight parts of the chains are shorter (several nm, typically, as one can conclude from the PL spectra). Long chains are fragmented into short straight arts because of the kinks clearly visible e.g. in Fig. S4 (c).

Being connected by carbon threads, gold nanoparticles having different work functions acquire polarization charges. The amount of charge redistributed between NPs is expected to be dependent on their sizes. In particular, two identical NPs, which are brought into contact or connected by a thin conducting wire, would not exchange electrons. On the other hand, if the metal spherical NPs are of different diameters (see fig. S6 (a) and (b)), the work functions of their electrons also differ.[20] Therefore, in order to bring the system into thermal equilibrium, the electrostatic energy of NPs must be changed to compensate the difference in their work functions. That is realized by transferring an electric charge between the NPs attached to different ends of the carbon chain. This charge exchange endows the NP-carbon wire complexes with the finite dipole moments and makes the linear chains of pollyne sensitive to the external electric field. This effect enables us to control the orientation of carbon chains at the stage of their surface deposition (see fig. S6(c)).

The ab-initio calculation results. The Density Functional Theory calculations for the infinite chain were performed using the QUANTUM ESPRESSO package.[21,22] We tested several exchange and correlation potentials: LDA, LSDA, PBE, PBE0, HSE06. An energy

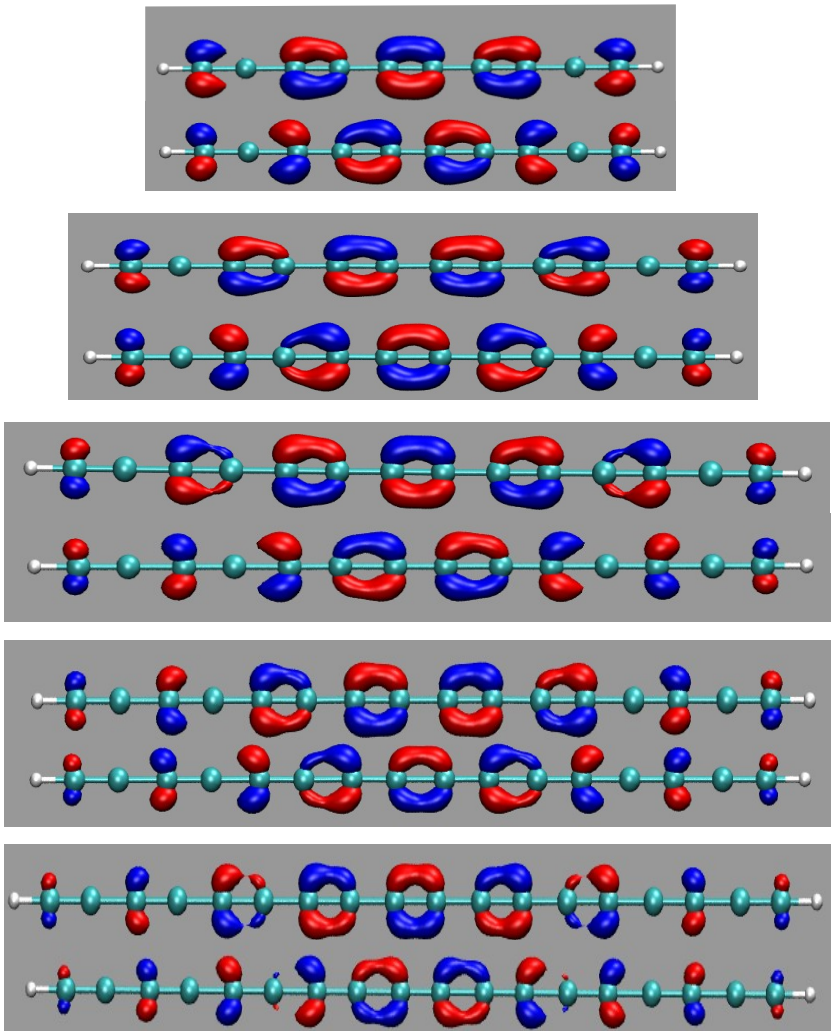

Figure S7: Molecular orbitals for C10, C12, C14, C16, C18 polyyne fragments. Top row: HOMO; Bottom row; LUMO. Red and blue lobes correspond to positive and negative values, respectively.

cutoff of 90 Ry and a k-points mesh of 16×1×1 k-points was used to optimize the atomic positions. A supercell with a vacuum of about 30 Å was employed, in order to avoid spurious interactions between neighbouring chains. We found that the polyyne geometry (that is, an infinite chain with single and triple bonds) can only be obtained with the use of hybrid pseudopotentials. In LDA, LSDA or PBE, instead, cumulene is the only stable structure,

with a zero electronic gap.

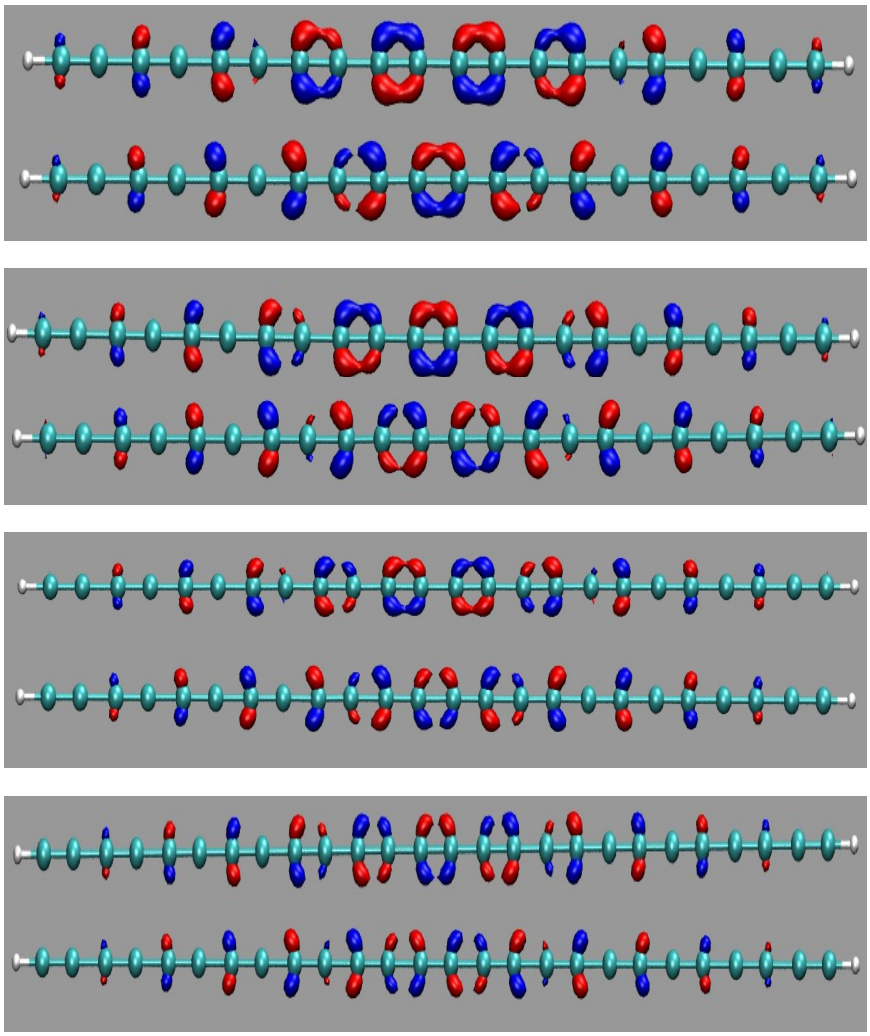

Figure S8: Molecular orbitals for C20, C22, C24 and C26 polyyne fragments. Top row: HOMO; Bottom row; LUMO. Red and blue lobes correspond to positive and negative values, respectively.

Optical spectra for varying lengths of the carbon chains (from 10 up to 26 C atoms) were obtained within Time Dependent Functional Theory (TDDFT) calculations with PBE0 kernel, using the code Gaussian[23] with triple-zeta 6-311+G(d,p) basis set plus LANL2DZ pseudopotential for gold core electrons,[24] after geometry optimisation. In all the considered cases, polyyne configurations have a lower energy than cumulene. The Density Functional Theory calculations for the carbon chain non stabilised with gold (H-terminated) were performed using the Gaussian 16 package, employing the PBE0 kernel with triple-zeta 6-311+G(d,p) basis

set. In the geometry-optimised chain (in polyyne configuration) one can see that HOMO and LUMO electron densities are spread over the whole chain in the absence of gold anchors at the ends.

The effect on the Carbon bond lengths of Au-nanoparticles, and the charge transfer between Au and C atoms, is shown in Tab.1 for the C14 chain. Results are compared with the C14 chain hydrogen-terminated. In agreement with the work,[25] a charge transfer occurs between C and the metal nanoparticles.

Table 1: The distances between adjacent C atoms in a C14 chain are reported here (d1-d13) for Au terminated and H terminated C chains. Also the partial charges q1–q14 are listed.

	d1	d2	d3	d4	d5	d6	d7	d8	d9	d10	d11	d12	d13	
Au	1.262	1.324	1.236	1.323	1.235	1.325	1.235	1.325	1.235	1.324	1.236	1.324	1.262	
H	1.211	1.351	1.222	1.339	1.227	1.335	1.228	1.335	1.227	1.339	1.222	1.351	1.211	
	q1	q2	q3	q4	q5	q6	q7	q8	q9	q10	q11	q12	q13	q14
Au	0.335	-0.220	0.078	-0.057	0.022	-0.019	0.005	-0.019	0.004	0.002	-0.043	0.073	-0.227	0.348
H	-0.320	0.111	-0.034	-0.001	-0.002	-0.012	0.000	-0.001	-0.011	-0.002	-0.000	-0.034	0.011	-0.320

References

(1) A. O. Kucherik, S. M. Arakelian, S. V. Garnov, S. V. Kutrovskaya, D. S. Nogtev, A. V. Osipov, and K. S. Khor'kov, Two-stage laser-induced synthesis of linear carbon chains, Quantum Electronics 46, 627 (2016).

(2) A. Kucherik, S. Arakelian, T. Vartanyan, S. Kutrovskaya, A. Osipov, A. Povolotskaya, A. Povolotskii, and A. Man'shina, Laser-induced synthesis of metalcarbon materials for implementing surface-enhanced raman scattering, Optics and Spectroscopy 121, 263270 (2016).

(3) N. Rozhkova, S. Rozhkov, and A. Goryunov, Natural graphene-based shungite nanocarbon, Carbon nanomaterials sourcebook: graphene, fullerenes,nanotubes and nanodiamonds 7, 151 (2016).

(4) H. Tammet, U. Hõrrak, and M. Kulmala, Negatively charged nanoparticles produced by splashing of water, Atmospheric Chemistry and Physics 9, 357367 (2009).

(5) G. Yangand C. X. Wang, Laser ablation in liquids: principles and applications in the preparation of nanomaterials, CRC Press, Ch.3 (2012).

(6) J.D. Buckley D.D. Edie, Carbon-Carbon Materials and Composites, Elsevier, 294 (1993) .

(7) P. Su, J. Wu, J. Gu, W. Wu, S. Shaik, and P. C. Hiberty, Bonding conundrums in the C^2-molecule: A valence bond study, Journal of Chemical Theory and Computation 7, 121130 (2010).

(8) B. Pan, J. Xiao, J. Li, P. Liu, C. Wang, and G. Yang, Carbyne with finite length: The one-dimensional sp carbon, Science Advances 1, 10.1126/sciadv.1500857 (2015).

(9) O. V. Yazyevand A. Pasquarello, Effect of metal elements in catalytic growth of carbon nanotubes, Physical Review Letters 100, 156102 (2008).

(10) T. Wakabayashi,H. Nagayama, K. Daigoku, Y.Kiyooka, K. Hashimoto, Laser induced emission spectra of polyyne molecules C_2nH_2 (n = 5–8), Chemical Physics Letters 446, 65 (2007).

(11) T. Wakabayashi, et al. Resonance Raman spectra of polyyne molecules C_10H_2 and C_12H_2 in solution, Chemical Physics Letters 433, 296 (2007).

(12) L. Shi, P. Rohringer, K. Suenaga, Y. Niimi, J. Kotakoski, J. C. Meyer, H. Peterlik, M. Wanko, S. Cahangirov, A. Rubio, Z. Lapin, L.Novotny, P. Ayala, T. Pichler, Conned linear carbon chains as a route to bulk carbyne, Nature Materials 15, 634639 (2016).

(13) Agarwal, N. R. et al. Structure and chain polarization of long polyynes investigated with infrared and Raman spectroscopy, J. Raman Spectrosc. 44, 1398 (2013).

(14) S. Kutrovskaya, I. Chestnov, A. Osipov, V. Samyshkin, I. Sapegina, A. Kavokin, A. Kucherik, Electric field assisted alignment of monoatomic carbon chains, Scientific Reports 10, 9709 (2020).

(15) Yu.P Kudravtsev et al, Oriented Carbyne Layers, Carbon 30, 213 (1992).

(16) A. M. Sladkov, Carbyne – the third allotrope of carbon, Nauka press, 79, (2003).

(17) V.M. Babina etc. Thermophysics of high temperatures 37, 573 (1999).

(18) R. G. Polozkov et al, Carbon nanotube array as a two-dimensional hyperbolic material: ab-initio study, Physical Review B 100, 235401 (2019).

(19) R. B. Heimann, S. E. Evsyukov, L. Kavan, Carbyne and Carbynoid Structures, Springer Netherlands, 446 (1999).

(20) C. R. Ma, J. Xiao, and G. W. Yang, Giant nonlinear optical responses of carbyne, J. Mater. Chem. C 4, 4692 (2016).

(21) P. Giannozzi, S. Baroni, N. Bonini, M. Calandra, R. Car, C. Cavazzoni, D. Ceresoli, G. L. Chiarotti, M. Cococcioni, I. Dabo, et al. QUANTUM ESPRESSO: a modular and open-source software project for quantum simulations of materials, Journal of physics: Condensed matter 21, 395502 (2009).

(22) P. Giannozzi, O. Andreussi, T. Brumme, O. Bunau, M. B. Nardelli, M. Calandra, R. Car, C. Cavazzoni, D. Ceresoli, M. Cococcioni, et al., Advanced capabilities for materials modelling with Quantum ESPRESSO, Journal of Physics: Condensed Matter 29, 465901 (2017).

(23) M. J. Frisch, G. W. Trucks, H. B. Schlegel, G. E. Scuseria, M. A. Robb, J. R. Cheeseman, G. Scalmani, V. Barone, G. A. Petersson, H. Nakatsuji, X. Li, M. Caricato, A. V. Marenich, J. Bloino, B. G. Janesko, R. Gomperts, B. Mennucci, H. P. Hratchian, J. V. Ortiz, A. F. Izmaylov, J. L. Sonnenberg, D. Williams-Young, F. Ding, F. Lipparini, F. Egidi, J. Goings, B. Peng, A. Petrone, T. Henderson, D. Ranasinghe, V. G. Zakrzewski, J. Gao, N. Rega, G. Zheng, W. Liang, M. Hada, M. Ehara, K. Toyota, R. Fukuda, J. Hasegawa, M. Ishida, T. Nakajima, Y. Honda, O. Kitao, H. Nakai, T. Vreven, K. Throssell, J. A. Montgomery, Jr., J. E. Peralta, F. Ogliaro, M. J. Bearpark, J. J. Heyd, E. N. Brothers, K. N. Kudin, V. N. Staroverov, T. A. Keith, R. Kobayashi, J. Normand, K. Raghavachari, A. P. Rendell, J. C. Burant, S. S. Iyengar, J. Tomasi, M. Cossi, J. M. Millam, M. Klene, C. Adamo, R. Cammi, J. W. Ochterski, R. L. Martin, K. Morokuma, O. Farkas, J. B. Foresman, and D. J. Fox, Gaussian, Gaussian 16, Revision A.03, Inc., Wallingford CT, 2016.

(24) P. J. Hay, W. R. Wadt, Ab initio effective core potentials for molecular calculations - Potentials for K to Au including the outermost core orbitals, J. Chem. Phys. 82(1), 299 (1985).

(25) A. Milani et al., Structure modulated charge transfer in carbon atomic wires, Scientific Reports 9, 1648 (2019)